Supplementary Information for

Spatiotemporal receptive fields of barrel cortex revealed by reverse correlation of synaptic input

Alejandro Ramirez[1,2], Eftychios A. Pnevmatikakis[2,3,4], Josh Merel[2,3,4], Liam Paninski[2,3,4], Kenneth D. Miller[1,2,3], and Randy M. Bruno[1,2]

1. Dept. of Neuroscience
2. Kavli Institute for Brain Science
3. Center for Theoretical Neuroscience
4. Dept. of Statistics

Columbia University, New York, NY, USA

Correspondence to randybruno@columbia.edu

Nature Neuroscience: doi:10.1038/nn.3720

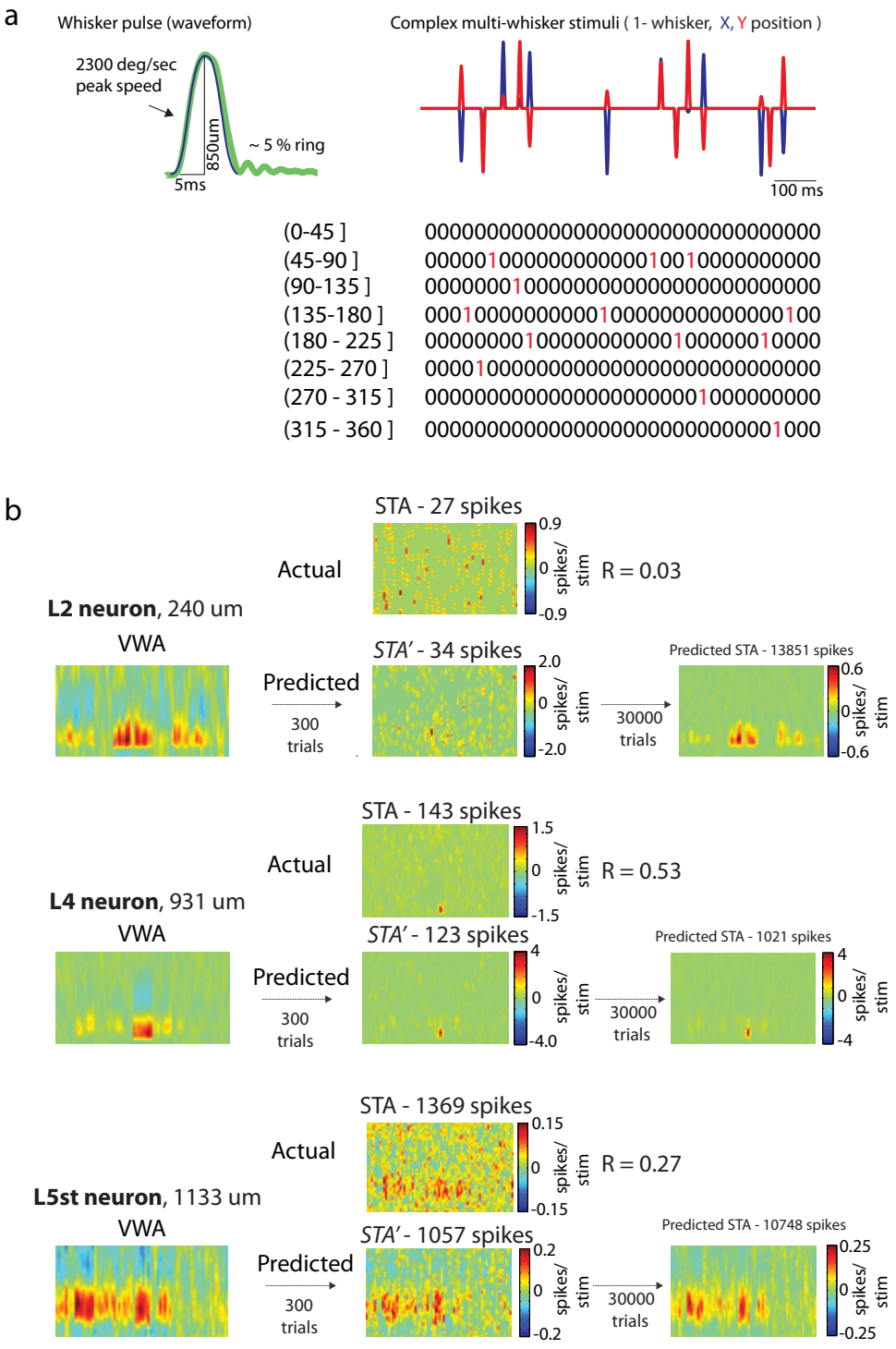

Supplementary Figure 1. Pulse waveform, stimulus representation, and example STA and STA'. a, An example of the waveform of individual pulse deflections (left) with the actual movement of the stimulator overlaid in green. The X,Y representation of movement for a single whisker for 1 second of complex stimuli (right). Below is a schematic of the binary representation of whisker movements for the same whisker in the 8-dimensional stimulus representation. Each whisker's state was represented in a given 1-ms time bin, where a 1 indicates the onset of a deflection in one of eight 45° bins. b, The VWA (left) for three example neurons is used to predict the STA' and compared to the actual STA (middle, and correlation coefficient). The model is also used to predict the STA' for 30000 extra trials of stimuli (right). For some neurons with low firing rates the STA-STA' correlation is low (top) and for some neurons with high firing rates the STA can be noisy (bottom). Nonetheless, for all neurons the VWA can be used to predict the STA' and has high correlation to the true STA (Fig. 1d,e).

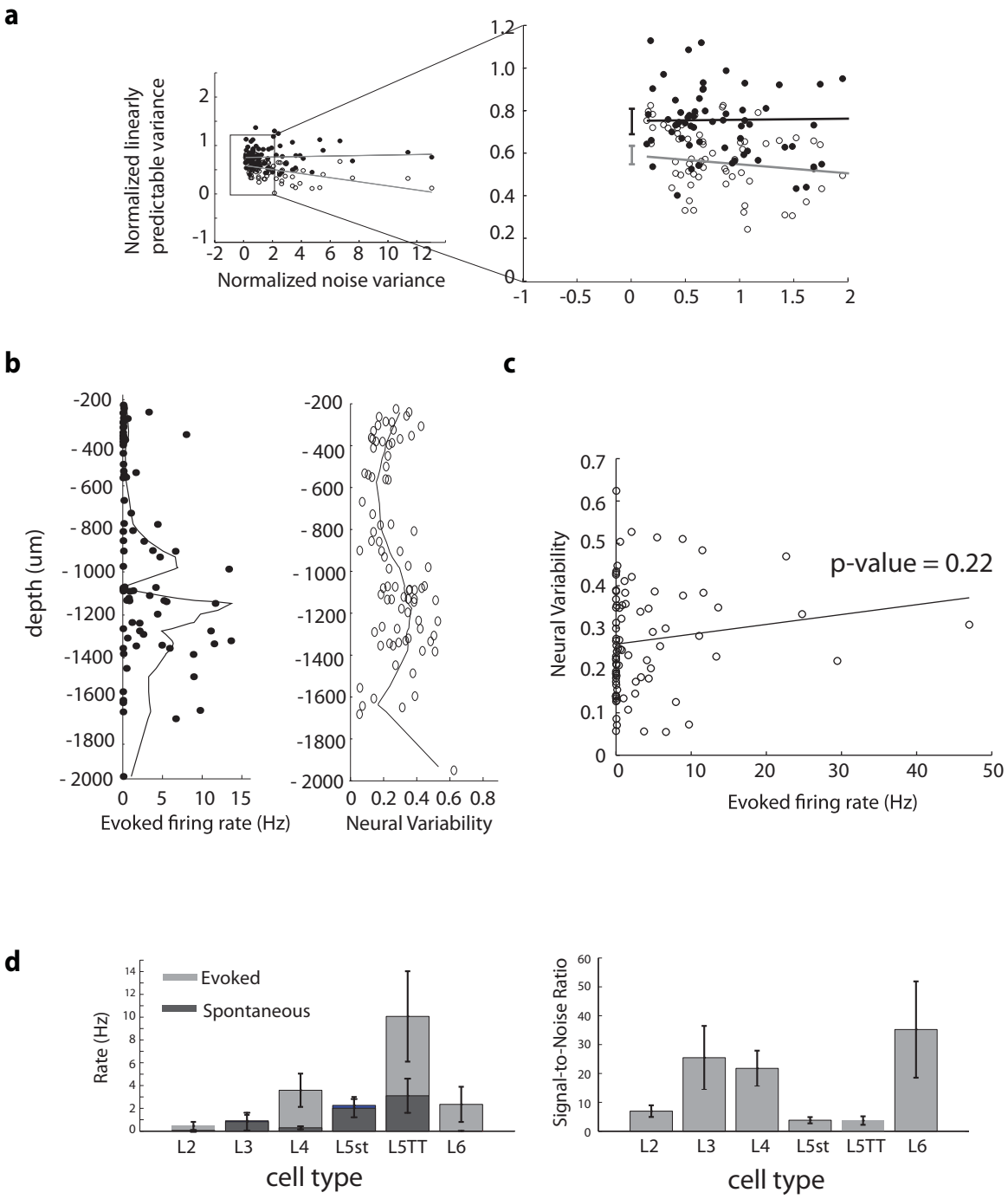

Supplementary Figure 2. Fraction of predictable variance accounted for by our model. Unbiased estimators of noise-related variance in our neural responses and the fraction of predictable variance accounted for by our model were calculated as in Sahani & Linden 2003. Black, training data. Gray, testing data. Extrapolating the performance of the model to conditions of zero noise gave an upper-bound of predictable variance of 0.75 ± 0.06 and a lower bound of 0.58 ± 0.03. b, The relationship between neural variability and firing rate. The firing rate is plotted by neuron and depth alongside a similar plot for variability by neuron and depth. c, There is no significant relationship between the firing rate and neural variability (right, p-value = 0.22). d, The firing rate (left) and signal-to-noise ratio, SNR (right), calculated as in Sahani & Linden 2003, are plotted by cell type. Neurons with high firing rates can have both low SNR (L5TT) or high SNR (L4) and neurons with low firing rates can have both low SNR (L2) as well as high SNR (L3 and L6).

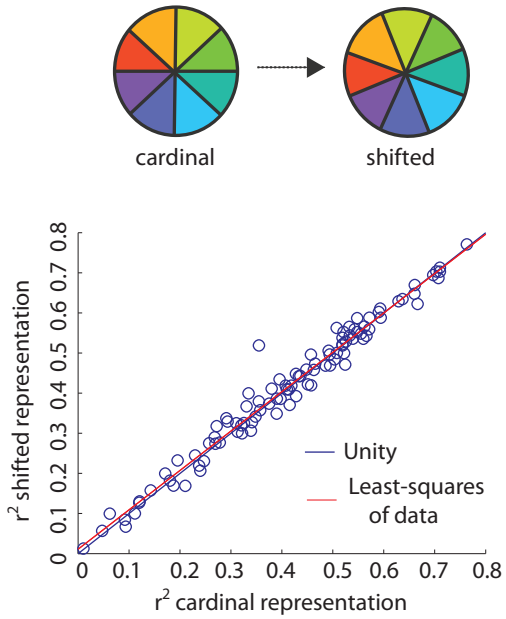

Supplementary Figure 3. Shifting the angle bins does not impair model performance. The 8-dimensional representation binned in cardinal directions (top left) was compared against one where the bins were shifted by 22.5° (top right). For each neuron, model performance using the cardinal stimulus representation was plotted against performance using the shifted representation (bottom). The least-squares regression of the data (red) falls exactly over the unity line (blue) demonstrating that cardinal directions play no special role and that this level of directional discretization (45° wide bins) used in our is adequate.

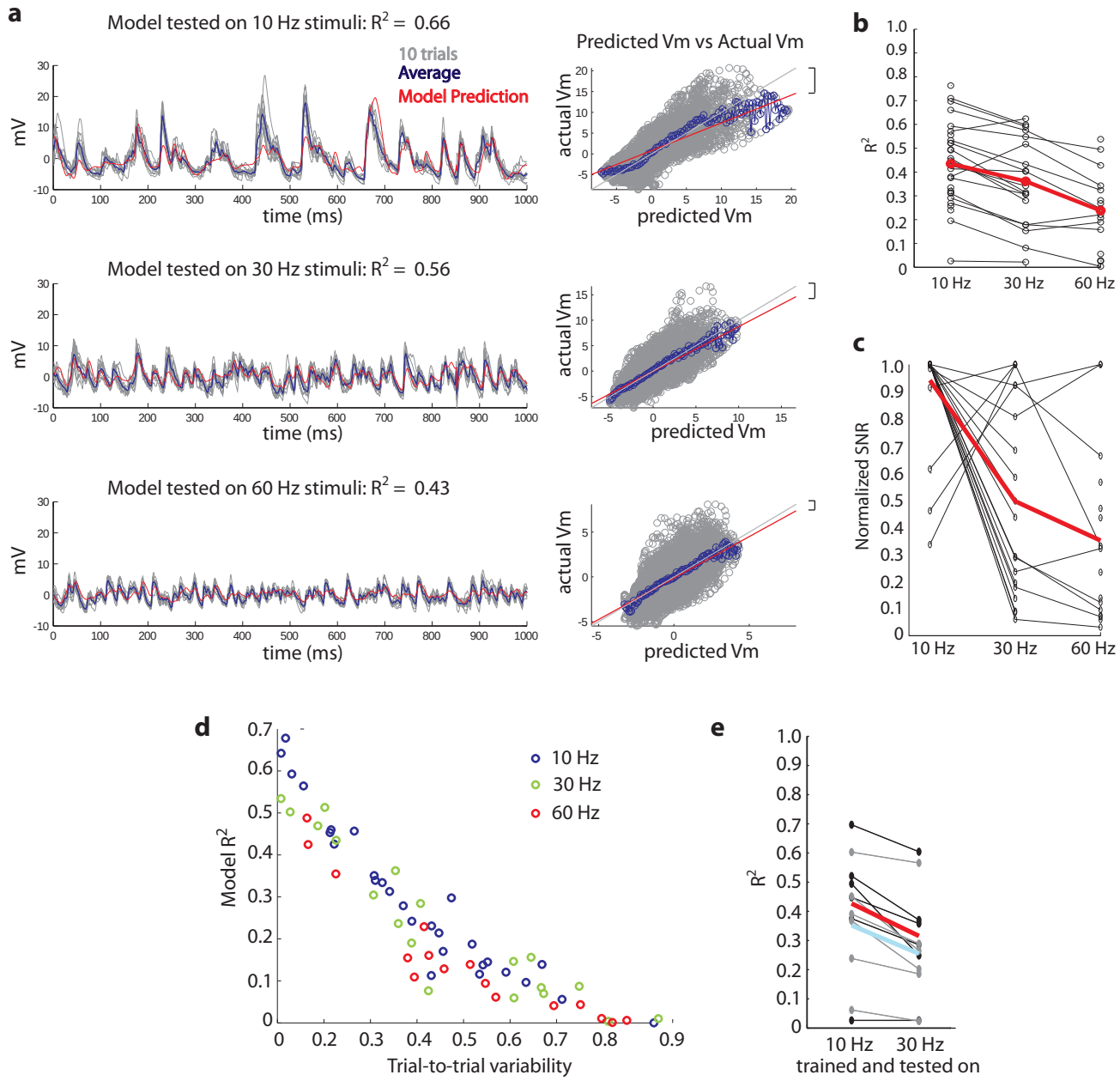

Supplementary Figure 4. Linearity is not dependent on stimulus frequency. A linear model was fit using our standard 10 Hz stimuli and then cross validated on 10, 30 and 60 Hz stimuli. a, an example neuron. For each plot on the left the gray traces illustrate ten trials of frozen noise, along with the average response (blue) and predicted response (red). On the right, the voltage predicted by our model is plotted against the actual voltage of the neuron for each 1-ms time bin (gray). Blue dots are the binned meaned data. The red line is the least-squares regression of the data, which can be compared to the unity line (gray). Although model performance (R^2) dropped as the frequency of stimulus increased from 10 to 30 to 60 Hz, the apparent linearity in fact increased (red line closer to unity, indicated by brackets). b, The R^2 for the model tested at 10, 30, and 60 Hz stimuli (N = 30 cells; not all three conditions were available for all neurons). There was a consistent drop in performance for almost all neurons as the frequency of whisker stimuli increased. However, c, the normalized signal-to-noise ratio (SNR) at 10, 30, and/or 60 Hz, as calculated in Sahani and Linden 2003, for the vast majority of cells dropped (both increased noise and decreased signal) as the frequency increases, explaining the drop in model performance seen in b. The neurons where the SNR increased in panel c were the same neurons where model performance also increased in panel b. d, To verify that the model was linearly dependent on the variability of the neuron and independent of stimulus frequency, we plotted the performance of the model against the trial-to-trial variability of the neurons (as in Fig. 2c). There was a similar relationship irrespective of whether models were tested on 10, 30, or 60 Hz stimuli. e. For a subset of neurons (N=5) we trained and tested the linear (black) and quadratic (gray) models at both 10 Hz and 30 Hz stimuli and compared the R^2 values. The linear model consistently outperformed the quadratic model, even at higher stimulus frequencies. The average of the linear model is shown in red and the average of the quadratic model is shown in cyan.

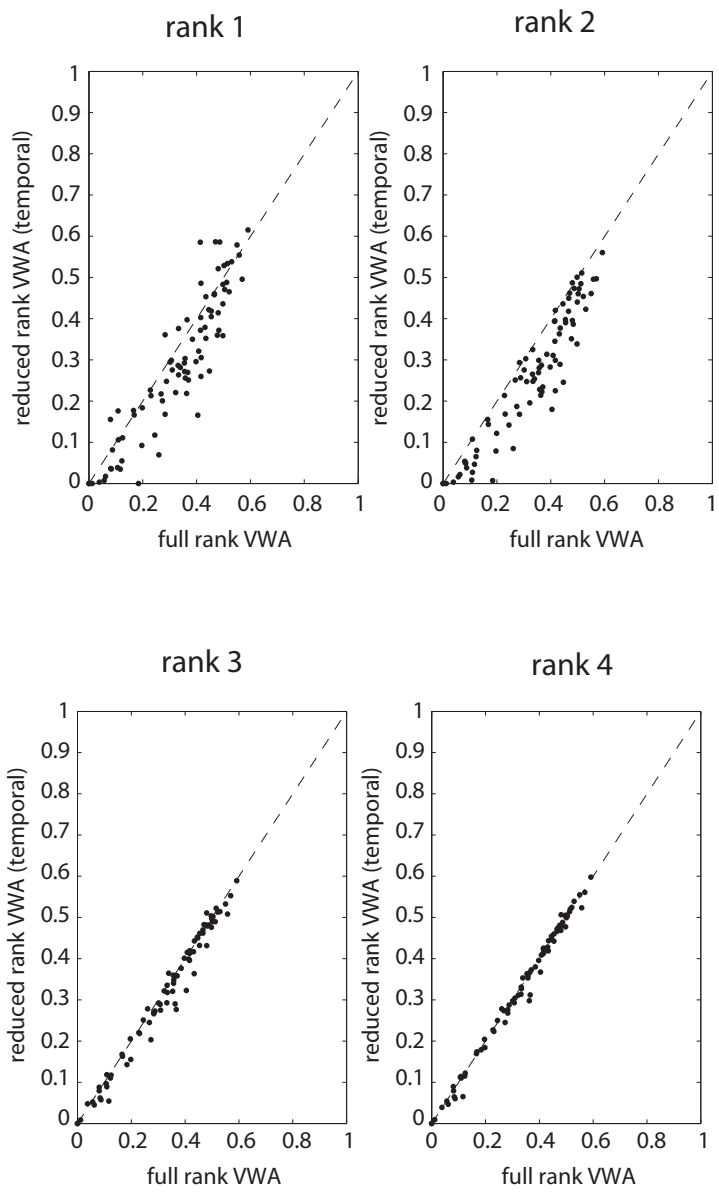

Supplementary Figure 5. Four temporal basis components are sufficient to describe the receptive fields of all neurons in the population. To find shared temporal basis components across neurons, we can simply stack the VWAs of all of the neurons together (to form a 100 by (72*N) matrix where N=number of neurons) and run singular value decomposition on this large matrix. The first few temporal components will be selected to allow for optimal squared error reconstruction of all of the VWAs. From left to right, the plots depict the predictive performance of various reduced rank models (reconstructed from 1 to 4 shared temporal basis components) against full rank models (100 temporal basis components). The rank refers to the rank of the RF matrices with temporal basis components shared across neurons. Critically, the temporal basis components are the same for all neurons, so the low number of components required to match full rank performance demonstrates that there is shared structure in the temporal components of the VWAs across all neurons. By rank 3, the low rank model predictive performance is approximately equivalent to the full rank model, demonstrating no more than 3 or 4 temporal basis components are required to capture the RFs of any neuron in the population.

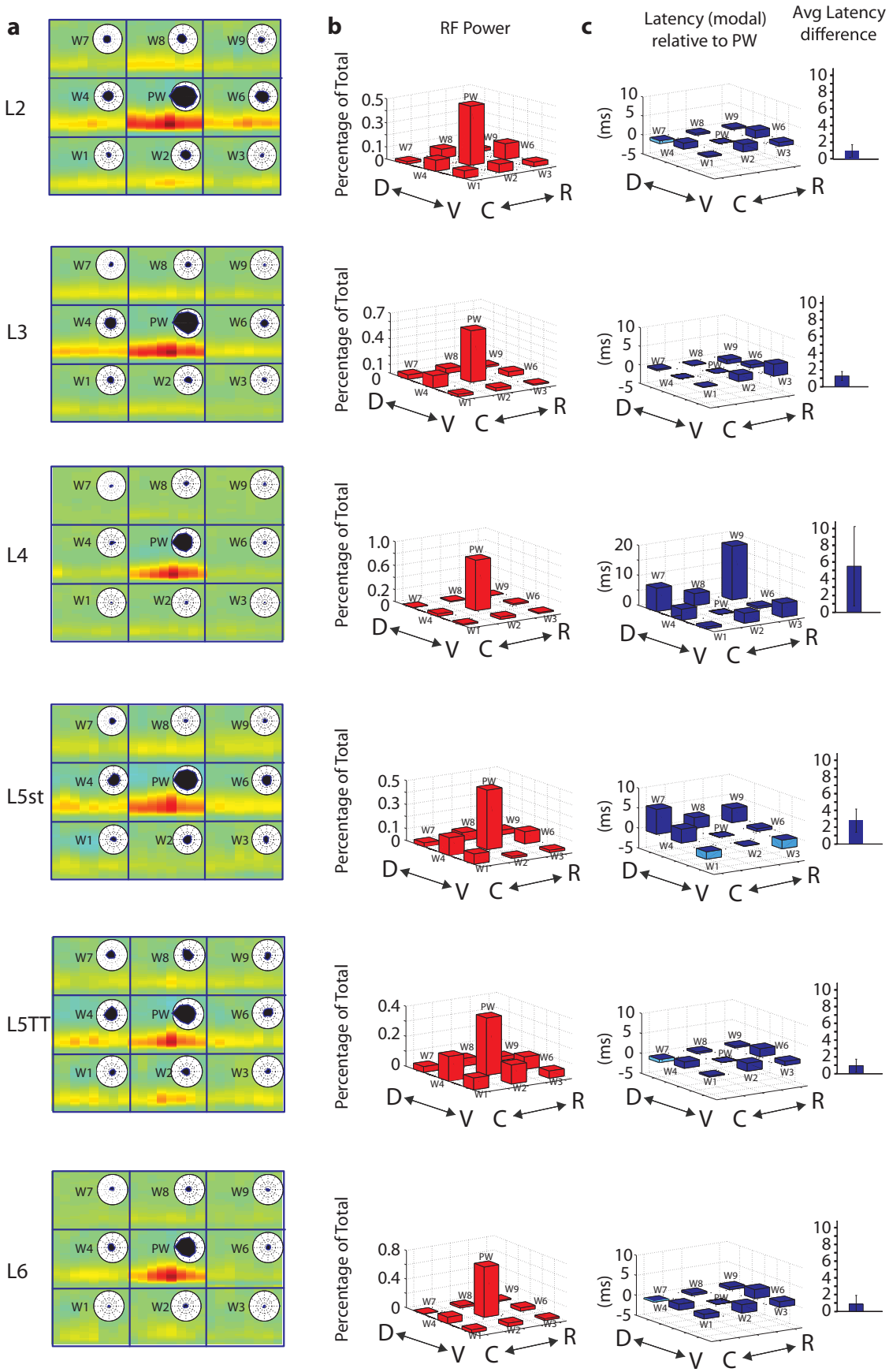

Supplementary Figure 6. Topological representation of STRFs. a, The average STRFs from Fig. 5a are represented in a manner that maintains the topological organization of the whiskers. The inset shows the polar plot of responses for each respective whisker. b, The fraction of power contained by each of the whiskers in the receptive field is plotted in order to show the spatial gradient of responses. c, The latency of surround whisker responses relative to the PW response are plotted according to whisker location and the average for all is plotted to the right to show the optimal inter-whisker latencies by layer and cell type.

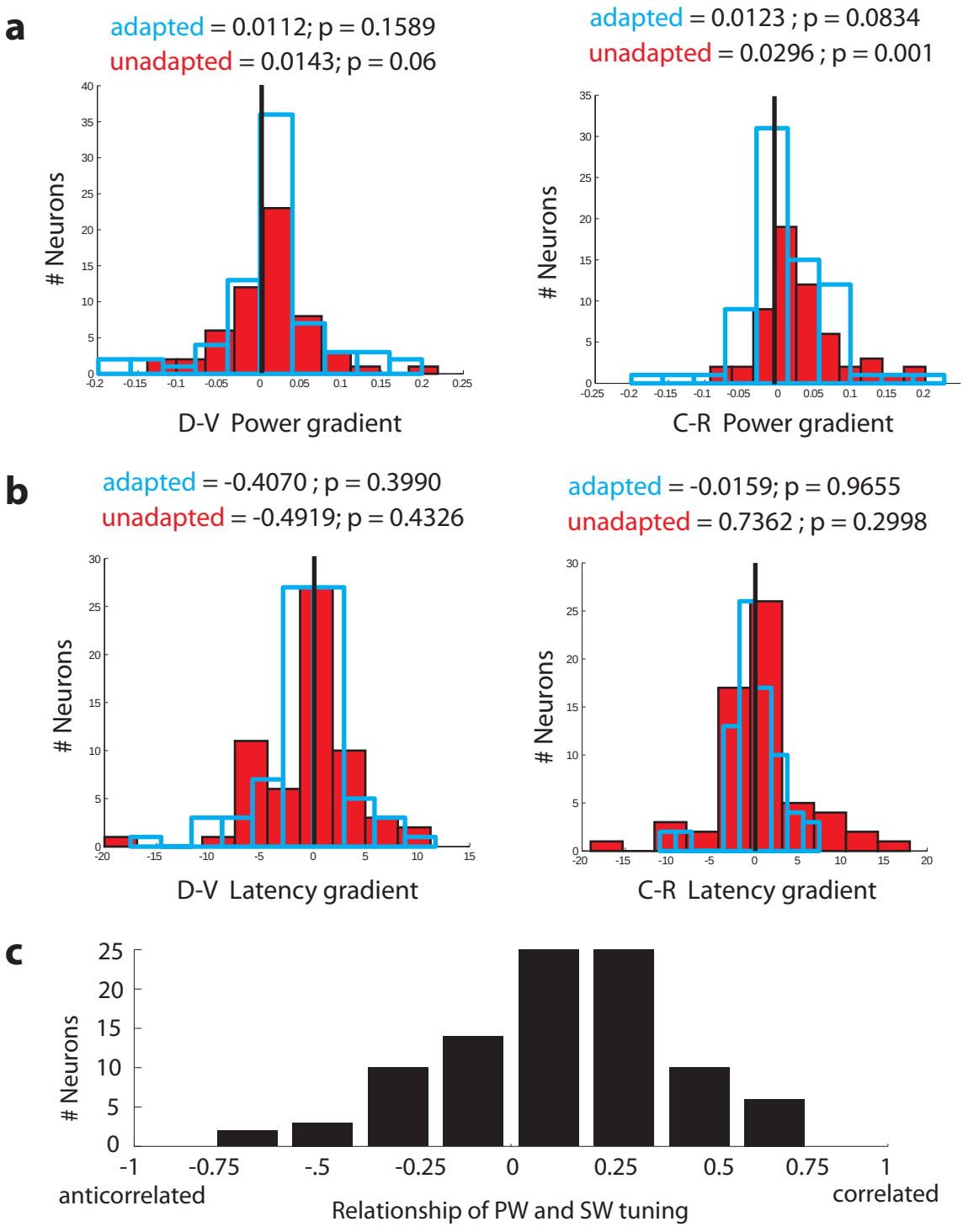

Supplementary Figure 7. Surrounds lack strong subthreshold spatial gradients but tend to have similar directional tuning to the principal whisker. a, For all neurons in either the adapted state (N = 71) or the unadapted state (N = 68), the dorso-ventral and caudal-rostral response gradients in the receptive fields were calculated as in previous studies (see Brumberg, Pinto & Simons 1996, Bruno & Simons 2002; i.e., ($Response_{dorsal}$ – $Response_{ventral}$) / ($Response_{dorsal}$ + $Response_{ventral}$)) and a histogram of responses was plotted for the dorso-ventral bias (left) and caudal-rostral bias (right). b, Spatial gradients of latency of the surround response were similarly calculated. c, The relationship of the PW and SW tuning was calculated, for each neuron, as the mean correlation of the PW and each significantly responding surround whisker. A value of 1 would indicate that the directional tuning of all significant SWs were identical to the directional tuning of the PW; -1 that the directional tuning of all significant SWs were opposite to that of the PW. Note that, while SWs tend to be tuned like the PW, many cells are oppositely tuned or uncorrelated.

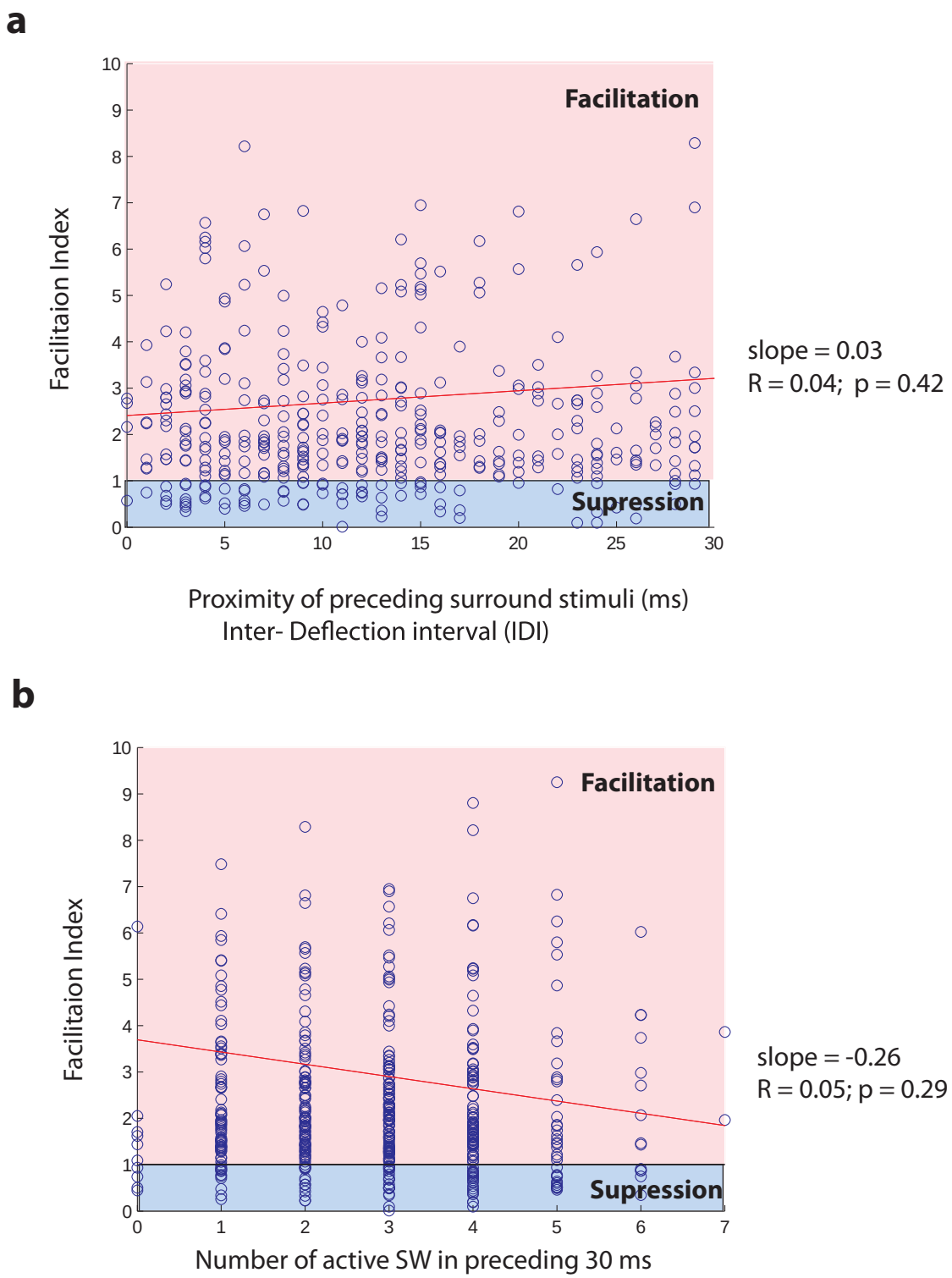

Supplementary Figure 8. Facilitation of adapted responses is independent of the precise nature of background stimuli. a, The facilitation index (the magnitude of the optimal multi-whisker response divided by the PW response, Opt PSP/PW PSP) does not depend on the proximity of the preceding background stimulus (p = 0.42). Each data point represents a single trial observation of the optimal stimulus. b, The facilitation index does not depend on the number of simultaneously active background inputs (p = 0.29).